Adsorption behavior of Sb(III) on iron-functionalized attapulgite in aqueous solution

Pengcheng Ni[a,b], Rui Zuo[a,b,*], Jinsheng Wang[a,b], Aixia Zhou[a,b]

aCollege of Water Sciences, Beijing Normal University, Beijing 100875, China, emails: zuo1101@163.com (R. Zuo), bnunpc2019@163.com (P. Ni), wangjs@bnu.edu.cn (J. Wang), zhouaixia2010@sina.com (A. Zhou)
bEngineering Research Center of Groundwater Pollution Control and Remediation, Ministry of Education, Beijing 100875, China

ABSTRACT

Sb, a toxic metal, exists widely in water and thus poses a serious environmental problem. This study presented the development of a novel and efficient iron-functionalized attapulgite (Fe-ATP) adsorbent, on which the adsorption behavior of antimony (Sb) from aqueous solutions was investigated. A variety of techniques, such as scanning electron microscopy, transmission electron microscopy, energy-dispersive X-ray spectroscopy, and Fourier-transform infrared spectroscopy, were used to characterize Fe-ATP. The influence of pH, temperature, and coexisting ions on adsorption was discussed. The results showed that the adsorption process reached equilibrium within 180 min at an initial Sb(III) concentration of 10 mg/L. The pH critically affected adsorption; the removal percentages were 92% and 62% at pH 4 and 13, respectively. The adsorption principles fitted the Freundlich model ($R^2 > 0.990$) and the pseudo-second-order model ($R^2 > 0.999$) well, indicating that the process was predominantly controlled by chemical processes. The enthalpy change of 6.5 kJ/mol and negative Gibbs free energy change indicated that adsorption was endothermic and spontaneous. It was also proven that the Fe-ATP was a recyclable adsorbent based on desorption experiments using ethylenediaminetetraacetic acid and NaOH solutions. The findings of the present work highlight the potential applicability of Fe-ATP as an effective sorbent for the selective removal of Sb(III) in water treatment processes.

Keywords: Antimony pollution; Iron-functionalized attapulgite (Fe-ATP); Adsorption; Wastewater

1. Introduction

Anthropogenic activities and industrial development have introduced many heavy metals to the lithosphere and biosphere, thus greatly pressuring the environment [1]. Sb is one of the most toxic and potentially carcinogenic heavy metals [2]. It occurs naturally in sulfide stibnite (Sb_2S_3), which is associated with As deposits [3]. Sb compounds have been extensively used in ammunition, battery grids, fire retardants, cable coverings, and pigments in paint and glass because of its specific properties [4]. It has been reported that 1.4×10^5 tons of Sb were utilized worldwide annually [5].

However, Sb released into the environment can destroy intracellular ion balances, causing damage to the nervous system and other organs [6]. Therefore, it is considered a priority controlled pollutant by the United States Environmental Protection Agency (USEPA), the Council of the European Communities (ECs), and the World Health Organization (WHO), which have defined maximum contamination levels in drinking water as 6, 10, and 5 µg/L, respectively [7].

As element in the same subgroup, the existence and chemical properties of Sb are similar to those of As [8]. It mainly exists in the Sb(V) and Sb(III) states in oxidizing and anoxic conditions, respectively. Sb(V) pollution of surface water and soil is usually caused by the oxidation of Sb(III) in Sb_2S_3 to Sb(V). However, Sb(III) is the favored form in anoxic environments, including groundwater and sediments,

* Corresponding author.

because of its slow oxidation rate [9]. Furthermore, Sb(III) is 10 times as toxic as Sb(V) [10]. Therefore, Sb(III) is the research objective of this work.

Regarding public health and environmental protection, it is highly urgent to develop advanced technology to address Sb as a pollutant. Many techniques for the removal of Sb from contaminated water have been investigated, such as coagulation [11], reverse osmosis [12], electrolytic reduction [13], ion exchange [14], membrane filtration [15], solvent extraction [16], and adsorption [17]. Thus far, adsorption is considered a good potential method to remove heavy metals because of its rapidness, effectiveness, and possibility for regeneration [18]. Previous works have demonstrated that the adsorption capacities of Sb on graphene [19] and polyamide-graphene [20] were 7.5 and 158.2 mg/g, respectively. Rakshit et al. [21] found that its adsorption on gibbsite was closely related to the pH. The adsorption of Sb(III) on carbon steel was significantly influenced by MoO_4^{2-} or SeO_3^{2-} [22]. Xi et al. [23] investigated the adsorption of Sb on goethite, reporting the equilibrium reaction time of 24 h. Although these adsorbents were successful in removing Sb in laboratory experiments, some problems remain in practical treatments. These adsorbents require exacting experimental conditions, such as limited pH variations or long equilibrium times. The natural reserves of materials for these adsorbents are relatively low and the costs are therefore high. The high cost of graphene in particular has limited its potential for large-scale removal of Sb.

Attapulgite (ATP) is an ideal candidate adsorbent material from environmental and economic perspectives [24]. ATP, which has the theoretical formula of $(Mg,Al)_4(Si)_8$ $(O,OH,H_2O)_{26} \cdot nH_2O$, is a natural hydrated Mg–Al silicate with a rod-like morphology formed in a specific geological environment [25,26]. Due to the rod-like crystal morphology, rich pores, large specific surface area, and negative surface charge, ATP has been widely used as a high-efficient adsorbent for the removal of various pollutants, such as metal ions [27,28], dyes [29], antibiotics [30], color matters [31], P [32], and humic acid [33]. However, natural ATP does not meet the requirements of current applications because of its limited adsorption capacity. Thus far, different modification technologies have been used to improve the adsorption capacity in recent years [34–38]. Fe oxides are widely considered as effective adsorbents for the removal of heavy metals by scientific researchers [39–43]. It is expected that nanoscale composites of iron oxides with ATP could improve the ability to remove Sb from the environment. However, literature regarding the modification of ATP with Fe is quite limited.

The objectives of this study are to synthesize and characterize iron-functionalized attapulgite (Fe-ATP), to investigate the ability of Fe-ATP to immobilize Sb(III) in aqueous solution, and to discuss the influences of pH and coexisting ions on the removal of Sb(III). According to the calculated isothermal, kinetic, and thermodynamic parameters of the adsorption process, the adsorption behavior of Sb(III) onto Fe-ATP is analyzed.

2. Materials and methods

2.1. Materials

The natural ATP used in this study was extracted from the Huangnishan Mine located in Xuyi County in Jiangsu Province, China. The chemical composition of ATP was determined by X-ray fluorescence spectroscopy (XRF), and the main oxides are shown in Table 1. In addition, the cation-exchange capacity of ATP was approximately 25–40 cmol/kg and the zeta-potential was −25.8 mV. The main associated minerals are quartz, mica, and montmorillonite. The collected ATP was air-dried and ground into powder. A stock solution of 100 mg/L Sb(III) was prepared from $SbCl_3$ (Merck, Darmstadt, Germany) and then diluted to the required concentrations. All reagents were purchased at analytical purity and employed without further purification. Double-distilled water (Beijing Jiulu Water Station, Beijing, China) was used throughout.

2.2. Preparation of Fe-ATP

The novel composite material of Fe-loaded ATP was prepared. Approximately 15 g of natural ATP powder and 0.45 g $(NaPO_3)_6$ as a dispersant were added to 200 mL deionized water in a 400-mL beaker under vigorous stirring for 30 min. The mixture was then sonicated for 1 h. The dispersion was centrifuged at 4,200 rpm and the remaining solid was vacuum-dried overnight at 60°C. Consequently, the purified solid was obtained by milling using a 100-mesh screen, yielding particles of approximately 0.15 mm in diameter.

According to the ratio (w/w) of 3% (Fe/ATP), approximately 5 g of purified ATP was dissolved in 250 mL deionized water; 0.724 g $FeCl_3$ (0.15 g Fe equivalent) was then dispersed in the mixed solution. The pH value of the mixture was adjusted to 9 by adding 0.1 mol/L NaOH solution. Then, the mixture was stirred at 30°C for 2 h. The aqueous suspension was centrifuged six times at 4,200 rpm for 10 min. The obtained solid was washed with deionized water until it was free of Cl⁻ in testing with $AgNO_3$ solution and then dried at 50°C until a constant weight was maintained. Finally, the Fe-ATP composite was sifted through a 100-mesh screen into a mortar and stored.

2.3. Adsorbent characterization

Morphological analyses were performed by scanning electron microscopy–energy-dispersive X-ray spectroscopy (SEM-EDS, Hitachi S-4800/EX-350, Suzhou, China).

Table 1
Chemical composition of ATP

Composition	Weight content (%)
SiO_2	52.29
Al_2O_3	8.86
Fe_2O_3	3.29
Na_2O	0.09
K_2O	0.78
CaO	2.67
MgO	17.70
MnO	0.13
TiO	0.33
LOI	13.86

LOI – loss on ignition.

A Tecnai G2 20 transmission electron microscope (TEM, FEI Company, USA) was employed to obtain TEM images. The specific surface area was determined by the Brunauer–Emmett–Teller (BET) method. The Fourier-transform infrared (FTIR) spectrum of each sample was recorded with a Nicolet Nexus 670 FTIR spectrometer (Nexus670, Nicolet, USA) to determine changes in the functional groups of the materials.

2.4. Batch adsorption experiments

The adsorption of Sb(III) on Fe-ATP was investigated by batch experiments. Approximately 50 mg Fe-ATP was dissolved in 25 mL of freshly prepared Sb(III) solution at a specified concentration. Then the mixture was shaken in a thermostatic reciprocating shaker at 150 rpm and 30°C. The pH of the solution was adjusted by adding negligible amounts of 0.1 mol/L HCl and/or NaOH solutions. After the suspension was shaken for 3 h, the liquid and solid phases were separated by centrifugation at 4,200 rpm for 10 min at 30°C. After the removal of Fe-ATP by filtration through 0.45-μm filter membranes, the concentration of Sb(III) in the supernatant was determined using an inductively coupled plasma atomic emission spectrometer (SPECTRO ARCOS EOP, SPECTRO Analytical Instruments GmbH, USA) under nebulizer flow conditions at 0.8 L/min. The limit of detection for Sb was 4 μg/L. In order to improve the accuracy, triplicate experiments were performed for each sample, and the final average values were used in calculation.

The removal percentage (%) and adsorption capacity (q_e, mg/g) were calculated with the following equations:

$$\% = \frac{C_0 - C_t}{C_0} \times 100\% \tag{1}$$

$$q_t = \frac{(C_0 - C_t)V}{m} \tag{2}$$

where C_0 and C_t represent the initial and final concentrations of Sb(III) in the solution (mg/L), respectively; V is the volume of the solution (mL); and m is the sorbent mass (mg).

3. Results and discussion

3.1. Material characterization

The SEM images were collected to confirm the morphology of Fe-ATP. No obvious changes on the surface between ATP (not shown) and Fe-ATP were observed from SEM images. As depicted in Fig. 1, the surface of Fe-ATP is uneven and shows rich pores, conducive to the adsorption of metal ions. The TEM images were collected to confirm the morphology of ATP and the prepared Fe-ATP. The circle in red indicates that the natural ATP has an intricate network-like structure with massive, regular rods (Fig. 2(a)). The networks of the purified ATP are more regular (Fig. 2(b)). It is reported that iron oxyhydroxide (FeOOH) is easily formed by mixing Fe^{3+} and NaOH solution with abundant Cl^- in the alkaline environment [44,45]. In this study, iron oxyhydroxide (FeOOH) composites (purple circle) are observed in Fe-ATP, suggesting that the modification process is successful (Fig. 2(c)). The Fe loading does not affect the overall rod-like structure of natural ATP, although the networks do become more compressed. Additionally, the BET specific surface area of ATP is 143 m^2/g, while that of Fe-ATP reaches 174 m^2/g. The pore structure of Fe-ATP is dredged, thereby improving the BET specific surface area.

EDS was used to reflect the distribution of elemental Fe. As shown in Fig. 3(a), Si, O, Ca, and Al are the major elements in Fe-ATP, and signals from Fe are observed in the EDS spectrum of Fe-ATP. The mapping of Fe in Fig. 3(b) indicates that Fe is evenly dispersed on Fe-ATP. Combined with the results of TEM analysis, we confirm that Fe is loaded on the surface of Fe-ATP. In order to determine the actual content of Fe loading on Fe-ATP, the elemental composition was determined by XRF. The weight content of Fe was calculated as 2.30% in natural ATP; this value increased to 3.76% after Fe modification.

The FTIR spectra obtained from ATP and the Fe-ATP composite are shown in Fig. 4. The bands at 3,615, 3,553, and 3,109 cm⁻¹ in the spectrum of ATP correspond to the stretching vibrations of Mg–OH units, Fe–OH units, and the bending vibration of water confined in zeolite, respectively. ATP exhibits a peak at 1,658 cm⁻¹ attributed to the bending vibration of
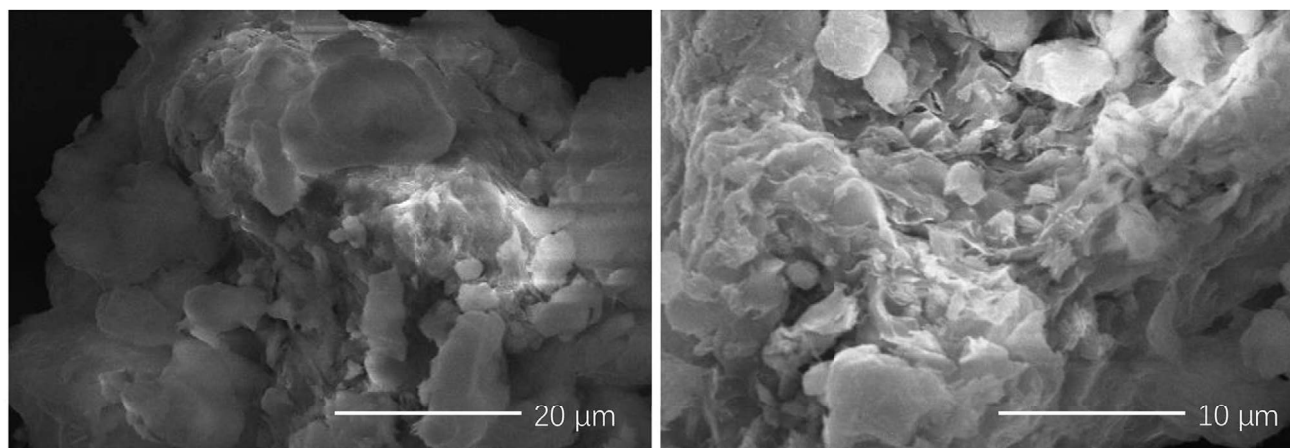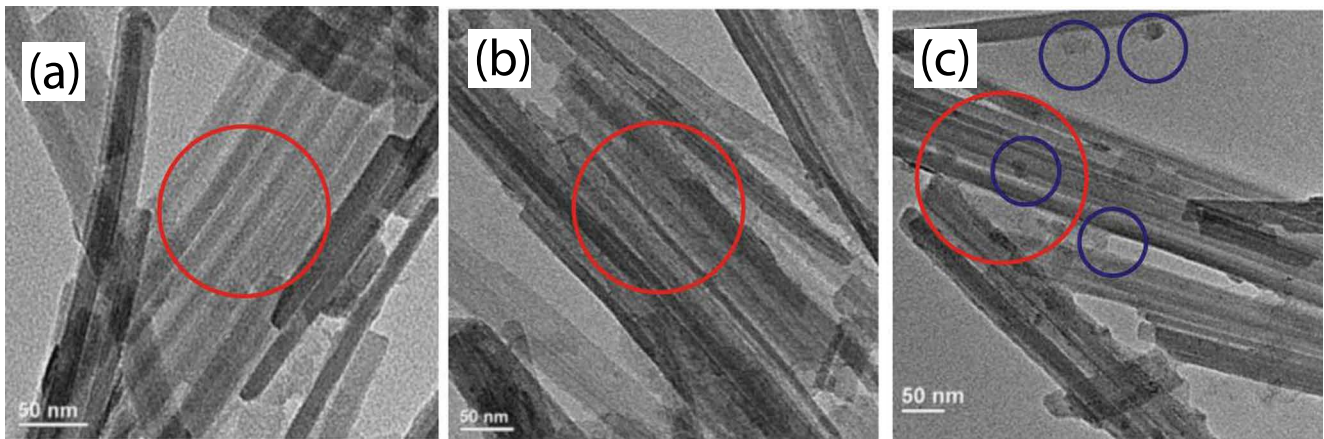

Fig. 1. SEM of Fe-ATP.

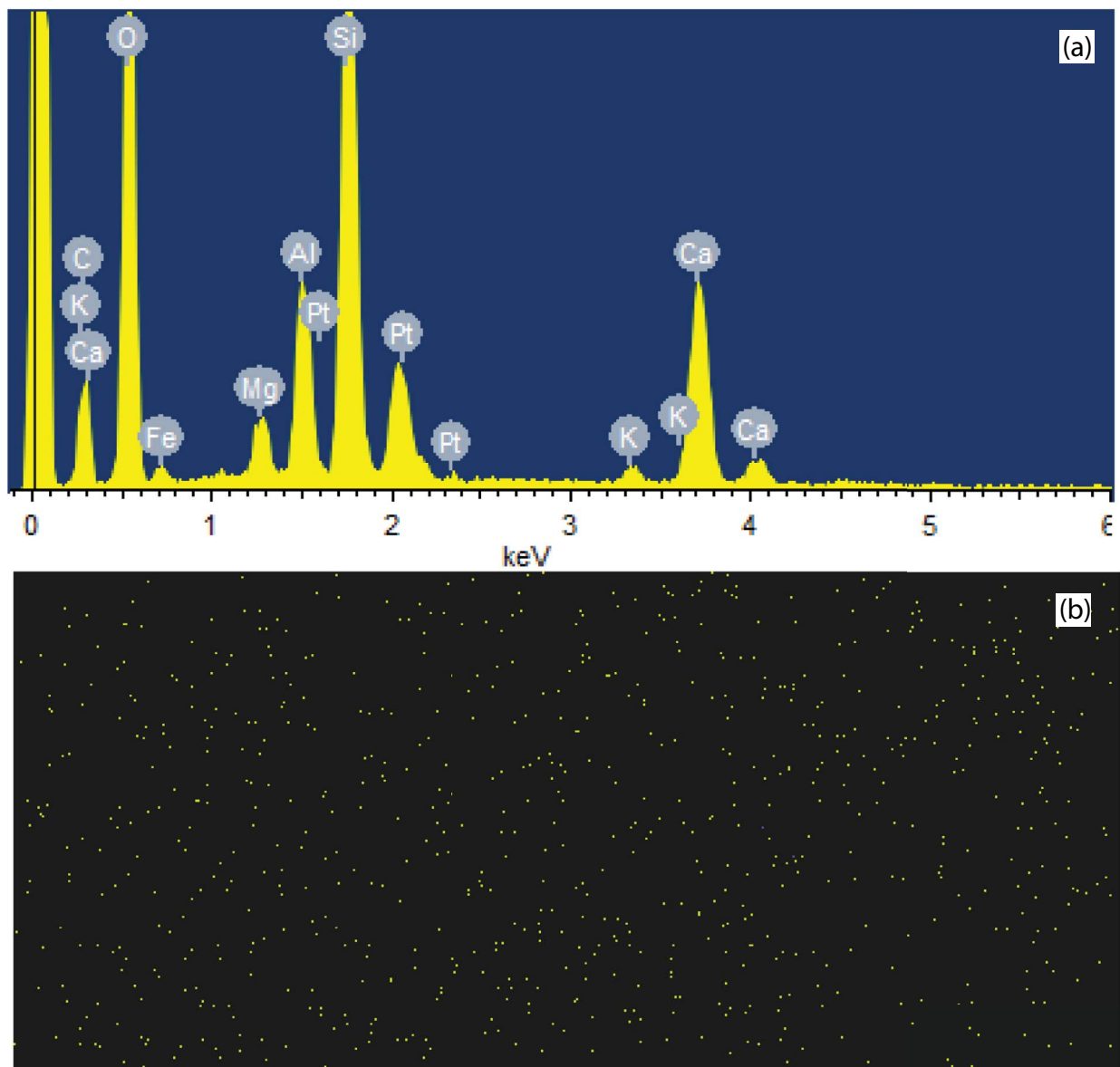Fig. 2. TEM of (a) ATP, (b) purified ATP, (c) Fe-ATP.

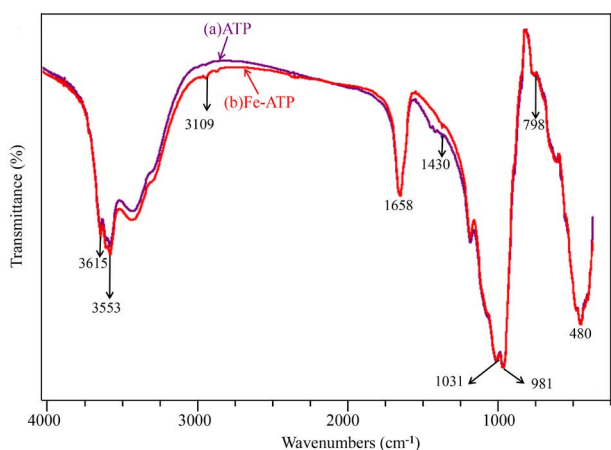Fig. 3. (a) EDS spectra of Fe-ATP and (b) the elemental mapping of Fe.

Fig. 4. FTIR spectra of (a) ATP and (b) Fe-ATP.

absorbed and coordinated molecular water [46]. The adsorption band ranging from 1,200 to 800 cm^{-1} is the strongest band observed from ATP. The bands at 1,031 and 981 cm^{-1} are attributed to the two different stretching vibrations of Si–O–Si. The appearance of these two peaks verifies that ATP is a silicate mineral. The bending vibrations of Si–O–Si for ATP are observed at 510 cm^{-1} and 476 cm^{-1}; in Fe-ATP, these are merged into one peak at 480 cm^{-1} because Si^{4+} is substituted by Fe^{3+}. The disappearance of the band at 1,430 cm^{-1} in the Fe-ATP spectrum reflects the decrease of CO_3^{2-} because of the reaction between Fe^{3+} and CO_3^{2-}. No obvious peaks are observed in the 2,000–3,000 cm^{-1} range in the spectrum. These results confirm again that Fe is successfully absorbed on the surface of ATP.

3.2. Sb adsorption experiments

3.2.1. Effect of pH on the adsorption

The pH of the solution is one of the most important factors controlling the adsorption process. It determines not only the surface functional groups on the adsorbent, but also the speciation of the metal ions in the solution [47].

The relationship between the speciation of Sb(III) and pH is shown in Fig. 5(a) [48].

The effect of pH on the removal percentage is presented in Fig. 5(b). In this study, for both ATP and Fe-ATP, the removal percentage is more than 60% throughout the tested pH range. The adsorption percentage gradually decreases with the increasing pH values at pH ranging from 5 to 13. High adsorptions of 82.63% and 92.46% for ATP and Fe-ATP are achieved at pH = 5, respectively. At acidic and neutral pHs, the removal percentages are relatively high. At pH < 3, $Sb(OH)_2^+$, SbO^+, and $Sb(OH)_3$ are the main species. The Fe^{3+} is released from Fe-ATP into the solution, which may cause coprecipitation with $Sb(OH)_2^+$ [11,49,50]. In addition, the cation exchange reaction between the silicate structure and H^+ induces a negative surface charge for Fe-ATP. The electrostatic attraction between $Sb(OH)_2^+$ and Fe-ATP thus promotes adsorption. At pH from 3 to 11, neutral $Sb(OH)_3$ and $HSbO_2$ are the principal species, accounting for more than 99% of the total Sb(III) in solution. The adsorption decreases slowly and reaches a plateau. For pH > 11.8, Sb(III) is present as SbO_2^-. At pH > 11, the removal percentage is decreased sharply; only 62% Sb(III) is adsorbed on Fe-ATP at pH = 13 because the surface charge of Fe-ATP becomes negative. Then the electrostatic repulsion between SbO_2^- and Fe-ATP impedes adsorption. Furthermore, hydroxylated complexes of Sb are formed and compete with the active surface bonds, inhibiting the adsorption percentage at higher pH [51]. Compared with natural ATP, Fe-ATP is more efficient for the removal of Sb(III). It is obvious that the Fe plays an important role for adsorption of Sb(III) on Fe-ATP.

The effect of pH on Sb(III) removal has been reported in other studies. The adsorption percentage of Sb(III) on Mn-modified perlite was 85% at pH = 4, while the adsorption yield was 40% at pH = 8 [51]. The removal percentage of Sb(III) on a magnetite surface in an aqueous organic acid environment was decreased with increasing the pH from 3 to 5.5 [49]. However, the results of Leng et al. [19] showed the increased removal percentage of Sb(III) by graphene as pH increased for pH > 4. The different pH effects observed for Fe-ATP and graphene are attributed to the domain function. Electrostatic factors mainly control the adsorption process in high-pH solutions for Fe-ATP, but not for graphene.
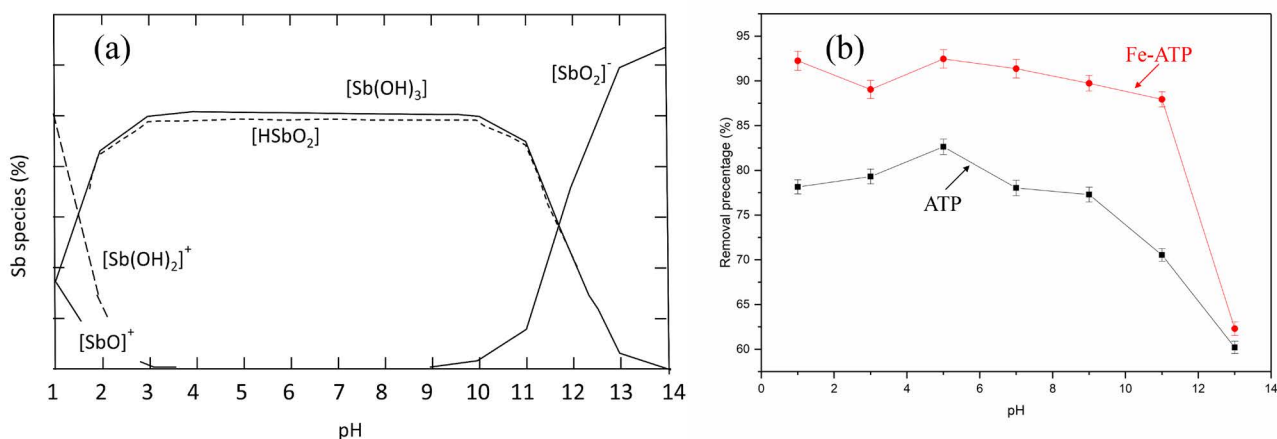

Fig. 5. (a) Sb species distribution at different pH ranges, (b) Effect of pH on the adsorption of Sb(III) on Fe-ATP (C_0 = 10 mg/L, T = 303 K, m = 50 mg, V = 25 mL, t = 180 min).

3.2.2. Effect of coexisting ions on adsorption

Because of the changes of the mobility and bioavailability of Sb(III), the adsorption process can be influenced by other ions present in Sb-contaminated water. For both natural surface water and groundwater, the concentrations of ions including K^+, Ca^{2+}, Mg^{2+}, SO_4^{2-}, CO_3^{2-}, and HCO_3^- are relatively high compared with others. For example, the total concentration of CO_3^{2-} and HCO_3^- is between 0.5 and 8×10^{-3} mol/L, and HCO_3^- is the main species at neutral pH [52]. Therefore, these above ions were chosen as representative competing ions and used in a series of adsorption experiments. The required ions were obtained from analytical reagent-grade salts (NaCl, KCl, $CaCl_2$, $MgCl_2$, Na_2SO_4, Na_2CO_3, and $NaHCO_3$).

The results of the adsorption experiments are illustrated in Fig. 6. It is clear that the cations K^+, Ca^{2+}, and Mg^{2+} have modest effects on the adsorption behavior. The effects of these cations for Sb(III) adsorption have not yet been reported, so their effects on the adsorption of Hg, another heavy metal, by ATP were used for comparison. Cui et al. [53] showed that the adsorption of Hg on a polyaniline/ATP composite was slightly influenced by K^+, Ca^{2+}, or Mg^{2+}. SO_4^{2-} has no discernable effect on removal. This is similar to the results for the adsorption of Sb(III) on hematite-modified magnetic nanoparticles, in which the removal was decreased by only 1% when the concentration of SO_4^{2-} was greatly increased to 10 mM [7]. Xi et al. [54] also reported that no noticeable effects of SO_4^{2-} were found on the adsorption of Sb(III) by bentonite. The removal percentage value in the presence of CO_3^{2-} or HCO_3^- is decreased by 5%. The competition of CO_3^{2-} or HCO_3^- at specific active adsorption sites may cause this decrease in removal percentage. A similar phenomenon was observed in the adsorption of phosphate on magnetic Zr–Fe oxide nanoparticles. The coexisting SO_4^{2-} showed a slight effect, while HCO_3^- impeded the phosphate adsorption process [55].

3.3. Adsorption thermodynamics

The adjacent molecular interaction and solubility can be affected by the temperature. Therefore, the adsorption process is closely related to the temperature. Adsorption thermodynamics parameters are important because they can provide critical information regarding the spontaneity and thermal nature of the adsorption process. Three fundamental thermodynamic parameters, including the standard Gibbs free energy $\Delta G°$ (kJ/mol), standard enthalpy change $\Delta H°$ (kJ/mol), and standard entropy change $\Delta S°$ (J/mol K), were determined for the adsorption of Sb(III) by Fe-ATP. These basic parameters were calculated by employing the following equations:

$$\Delta G° = -RT \ln K_D \tag{3}$$

$$\Delta G° = \Delta H° - T\Delta S° \tag{4}$$

$$\ln K_D = \frac{\Delta S°}{R} - \frac{\Delta H°}{RT} \tag{5}$$

$$K_D = \frac{q_e}{C_e} \tag{6}$$

where R is the gas constant (8.314 J/mol K) and T is the temperature (K).

The effect of temperature on the adsorption of Sb(III) ions onto the Fe-ATP is shown in Fig. 7. The calculated values of $\Delta G°$ are −21.9, −22.9, and −23.8 kJ/mol at 303, 313, and 323 K, respectively. According to the negative $\Delta G°$ values, the adsorption process is spontaneous. It is clear that the process is mainly controlled by chemical processes based on the $\Delta G°$ values more negative than −20 kJ/mol [56]. Furthermore, the decrease of the negative $\Delta G°$ values with increasing temperature shows that the adsorption process becomes more favorable at higher temperatures. The values of $\Delta H°$ and $\Delta S°$ are 6.5 kJ/mol and 93.9 J/mol K based on the slope and intercept of the plot of $\ln K_D$ versus $1/T$, respectively. The positive value of $\Delta H°$ further demonstrates that the adsorption process is endothermic, which is confirmed by the increase of the K_D value with increasing temperature [57].
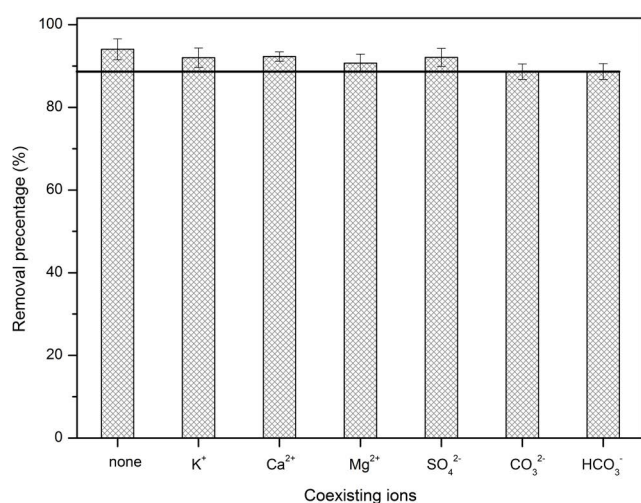

Fig. 6. Effect of coexisting ions on the adsorption of Sb(III) on Fe-ATP ($C_0 = 10$ mg/L, $T = 303$ K, $m = 50$ mg, $V = 25$ mL, $t = 180$ min).
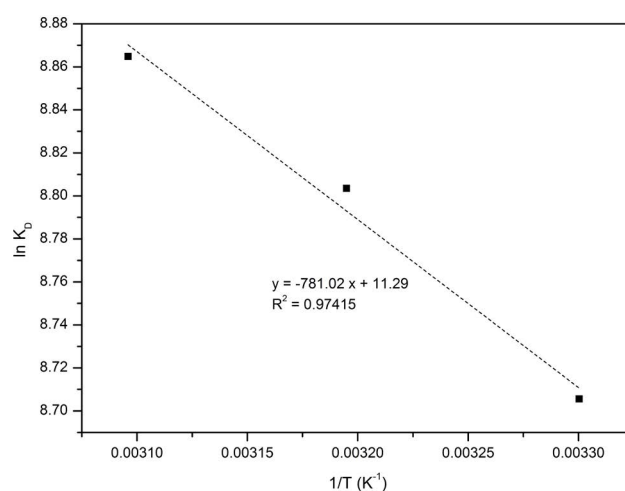

Fig. 7. $\ln K_D$ versus $1/T$ plot, used in the determination of thermodynamic parameters for the adsorption of Sb(III) on Fe-ATP.

Moreover, the positive value of $\Delta S°$ indicates the increase in the degrees of freedom of the adsorbed species.

Other studies on the adsorption thermodynamics of Sb(III) are found in the literature. The similar value of $\Delta G°$ (−16.5 kJ/mol) for the adsorption of Sb(III) by Mn-modified perlite was reported [51], and the process of Sb(III) on goethite was also spontaneous based on the negative value of $\Delta G°$ [48]. In this work, the adsorption process is endothermic according to the positive $\Delta H°$ value. However, Xi et al. [54] stated that the adsorption of Sb(III) on bentonite was exothermic, with the $\Delta H°$ value of −2.4 kJ/mol. It can be concluded that the adsorption process of Sb(III) on Fe-ATP absorbed energy, but that on bentonite releases energy. The differences between adsorption on Fe-ATP and bentonite are caused by the different adsorption mechanisms. The adsorption is influenced by the strength and energy of interactions between Sb(III) and the adsorbents. The former reaction is mainly controlled by chemical processes, while the latter proceeds physically.

3.4. Adsorption isotherm models

In order to investigate the surface properties and affinity of the proposed adsorbent, the obtained data were fitted with three important adsorption isotherm models of the Langmuir, Freundlich, and D–R isotherms. The relative viabilities of these models for the data were determined by the correlation coefficients (R^2) from fitting the data points using the least-squares method.

The Langmuir model depicts monolayer adsorption over a surface. It assumes that all adsorption sites have equal solute affinities and that no transmigrating sorbate exists in the surface plane. The model can be described using the following expression:

$$\frac{1}{q_e} = \frac{1}{q_m k_l C_e} + \frac{1}{q_m} \tag{7}$$

where q_e is the amount of Sb(III) absorbed on Fe-ATP (mg/g), C_e is the equilibrium concentration of Sb(III) in solution (mg/L), q_m is the maximum amount of Sb(III) absorbed on Fe-ATP (mg/g), and k_l is the Langmuir constant. The maximum amount of adsorbed Sb(III) is 9.54 mg/g and R^2 is 0.77596 (Fig. 8(a)). This relatively low R^2 value suggests that the relationship between q_e and C_e is not satisfactorily described by the model.

The Freundlich isotherm describes heterogeneous adsorption and the exponential distribution of active sites with different energies. This model can be expressed using the equation:

$$\ln q_e = \ln K_F + \frac{1}{n} \ln C_e \tag{8}$$

where the constant K_F, is related to the adsorption capacity and $1/n$ is an indicator of the adsorption intensity. While adsorption is prone to occur for $0.1 \leq 1/n \leq 0.5$, it is unlikely for $1/n > 2.0$. The Freundlich isotherm is suitable in describing the intermediate concentration range and unsatisfactory for high coverage.

As depicted in Fig. 8(b), the Freundlich isotherm model fits the data well with an R^2 value of 0.99045. The value
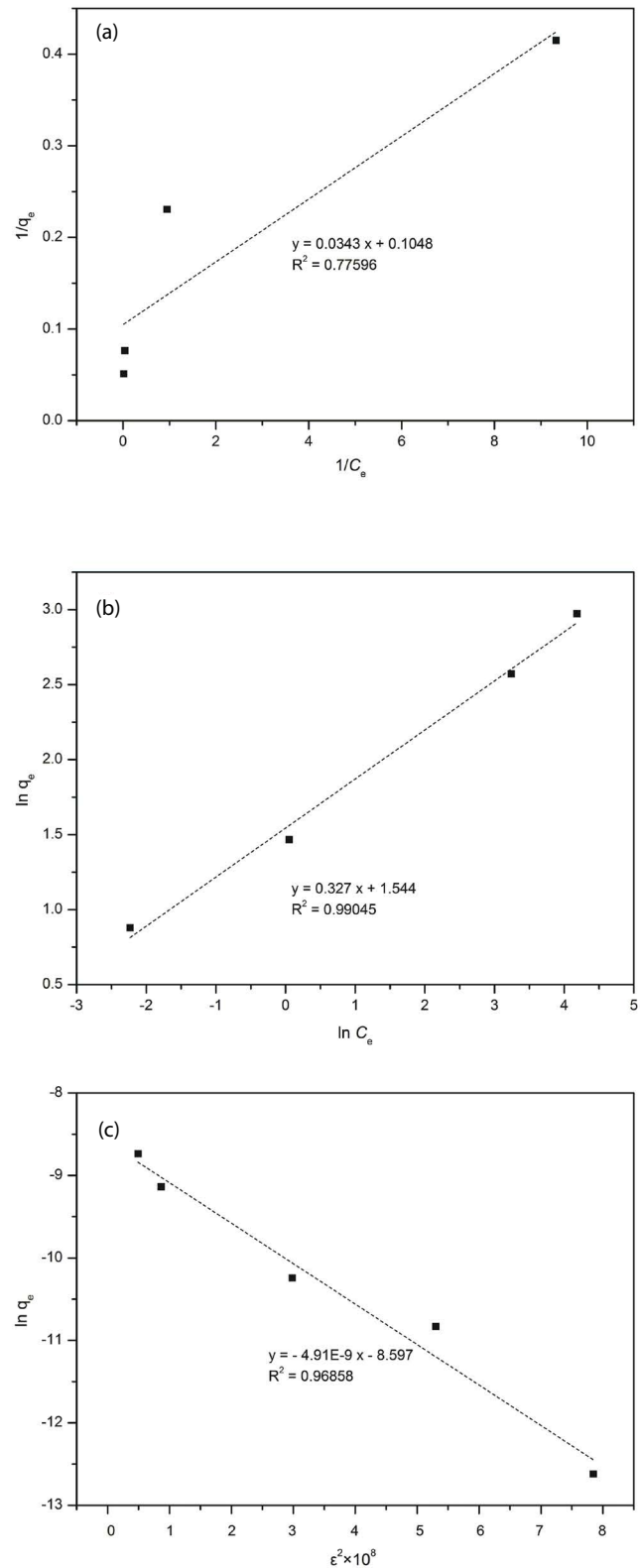
Fig. 8. Isotherm models obtained for the adsorption of Sb(III) on Fe-ATP: (a) Langmuir isotherm, (b) Freundlich isotherm, (c) D–R isotherm.

(0.327) of $1/n$, between 0.1 and 0.5, indicates that the adsorption of Sb(III) on Fe-ATP is favorable in the studied conditions. It also indicates that Sb(III) is adsorbed on Fe-ATP by multilayered active sites with different affinities toward Sb(III). Similar results have been reported in previous work. Xi et al. [54] presented the $1/n$ value for Sb(III) adsorption on bentonite of 0.923 at 298 K, while that for Sb(III) adsorption on goethite was 0.728 [48]. Sb(III) is more easily adsorbed on Fe-ATP than on bentonite or goethite, according to the lower $1/n$ value found in this work.

The D–R isotherm is more general than the Langmuir isotherm and is applied to analyze the nature of the Sb(III) adsorption process onto Fe-ATP as physical or chemical. The linear form of the D–R is written as follows:

$$\ln q_e = \ln q_m - \beta \varepsilon^2 \tag{9}$$

where q_e is the saturation capacity (mol/g); β is the activity coefficient (mol²/J²); and ε is the Polanyi potential, which can be calculated as follows:

$$\varepsilon = RT \ln \left(1 + \frac{1}{C_e} \right) \tag{10}$$

R is the universal gas constant (8.314 J/mol·K), T is the temperature (K), and C_e is the Sb(III) concentration in solution (g/L).

The q_m and β values are 1.85×10^{-4} mol/g and 5×10^{-9} mol²/J² based on the intercept and slope, respectively (Fig. 8(c)).

The mean free energy E (J/mol) is related to the constant β and can be obtained from the following equation:

$$E = \frac{1}{\sqrt{2\beta}} \tag{11}$$

The adsorption mechanism can be categorized as chemical adsorption, ion exchange, or physical adsorption depending on the attraction between the adsorbent and adsorbate. The value of E provides information on the adsorption mechanism. If E is smaller than 8 kJ/mol, the adsorption is physical in nature. For E of 8–16 kJ/mol, the adsorption occurs by chemical ion exchange. The adsorption occurs chemically for E exceeding 16 kJ/mol. In this work, the value of E is 10 kJ/mol, indicating that the adsorption of Sb(III) onto Fe-ATP progresses primarily via chemical ion exchange.

The D–R model has also been discussed for adsorption in previous work. Fan et al. [58] found the adsorption of Sb(III) on mercapto-functionalized hybrid sorbent was a chemical process according to the value of E (18.9 kJ/mol); in addition, the value of E was calculated at 6.3 kJ/mol for the adsorption of Sb(III) on Mn-modified perlite [51].

As seen from Table 2, in conclusion, the R^2 value (0.99045) of the Freundlich model is the highest among the values obtained relative to those from the Langmuir (0.77596) and D–R equations (0.96858). This demonstrates that the Freundlich isotherm fits the experimental data the best. Sb is easily adsorbed by Fe-ATP based on the value of $1/n$ (0.327). Adsorption capacity is a crucial factor to explore the adsorption ability of an adsorbent. The maximum capacity (q_m) is usually obtained from the adsorption isotherm model. It is clear that Freundlich equation is the best model to describe the adsorption behavior in this study. However, this equation does not contain the parameter of "q_m." Then compared with Langmuir equation, the D–R equation could describe it better. For this reason, the values (22.52 mg/g) of q_m from D–R model are considered as the maximum capacity for Fe-ATP.

The comparison of adsorption capacity of Fe-ATP with other adsorbent reported in literature is illustrated in Table 3.

Table 3
Comparison of Sb(III) adsorption capacity on Fe-ATP with that of different adsorbents

No.	Adsorbent	Adsorption capacity (mg/g)	Reference
1	Diatomite	35.2	[59]
2	Chemically bonded adsorbent	21.92	[60]
3	Goethite	61.5 (average)	[48]
4	Hydrous oxide of Mn	17.05	[62]
5	Hydrous oxide of Fe	12.18	[62]
6	MNP@hematite	36.7	[7]
7	Commercial Fe₃O₄	19.9	[7]
8	MWCNTs	0.33	[66]
9	Cyanobacteria *Microcystis* biomass	4.88	[68]
10	Fe₂O₃-modified CNTs	6.23	[70]
11	Graphene	8.056	[19]
12	Polyamide-graphene	158.2	[20]
13	Mn-modified perlite	76.5	[51]
14	Natural perlite	54.4	[51]
15	Imprinted polymer	6.7	[61]
16	Bonded silica gel	7.9	[63]
17	Sb(III)-imprinted sorbent	27.7	[64]
18	Nonimprinted sorbent	13.6	[64]
19	Green marine macroalgae	2.1	[65]
20	Brown seaweed	5.4	[67]
21	Sb(III)-imprinted silica gel	32.4	[69]
22	Nonimprinted sorbent	11.1	[69]
23	ATP	4.13	This study
24	Fe-ATP	22.52	This study

Table 2
Isotherm parameters for the adsorption of Sb onto Fe-ATP

Langmuir model			Freundlich model			D-R model		
q_m (mg/g)	K_L (L/mg)	R^2	K_F (mg/g)	$1/n$	R^2	q_m (mg/g)	β	R^2
9.54	3.06	0.77596	4.68	0.327	0.99045	22.52	5×10^{-9}	0.96858

Because of the different experimental conditions, the comparison results may be not extremely accurate. Though, it can be seen that the adsorption capacity of Sb(III) on Fe-ATP was better than some other adsorbents in some ways. In addition, compared with some other adsorbents, the adsorption reaction of Fe-ATP is very rapid and reaches equilibrium within 180 min. One of the great advantages for Fe-ATP is the rich reserve and low cost, making it more competitive in practical applications for wastewater treatment.

3.5. Adsorption kinetics

The effect of the contact time on the removal percentage of Sb(III) and capacity q_t is shown in Fig. 9(a). It is clear that the removal percentage increases with time. The adsorption rapidly increases as a function of time up to 180 min and slowly increases thereafter. The removal percentage and capacity are approximately 88% and 4.28 mg/g at 180 min, respectively. Xi et al. [54] reported that adsorption equilibrium for Sb(III) on bentonite was reached within 24 h. The adsorption of Sb(III) onto graphene reached equilibrium after 4 h [19]. Therefore, compared with other materials, Fe-ATP is more favorable for application in the removal of Sb(III) from large volumes of solution.

The adsorption kinetics can predict the rate of Sb(III) removal from aqueous solutions and provide valuable information on the adsorption mechanism. In order to clarify the adsorption kinetics of Sb(III) on Fe-ATP, pseudo-first-order and pseudo-second-order kinetics were investigated in this study.

The linear form of the pseudo-first-order equation can be written as follows:

$$\ln\left(q_e - q_t\right) = \ln q_e - k_1 t \tag{12}$$

where q_e and q_t are the amount of Sb(III) adsorbed onto Fe-ATP at equilibrium and at time t (mg/g), respectively; and k_1 is the rate constant, which is determined from the slope of the $\ln(q_e - q_t)$ versus t plot.

The pseudo-second-order model assumes that the rate is the limiting factor of the chemical adsorption mechanism. The equation is given as follows:

$$\frac{t}{q_t} = \frac{1}{k_2 q_e^2} + \frac{t}{q_e} \tag{13}$$

where q_e and q_t are the amount of Sb(III) adsorbed onto Fe-ATP at equilibrium and time t (mg/g), respectively; and k_2 is the rate constant. There is a negative correlation between the adsorption rate and the k_2 value.

Fig. 9 and Table 4 show the kinetic parameters of the pseudo-first-order and pseudo-second-order models at different temperatures. For the pseudo-first-order model, the R^2 values are low and the obtained q_e values (0.24–0.33 mg/g) differ greatly from the experimental data. It is clear that the pseudo-first-order model is inappropriate for modeling the adsorption process. However, the high R^2 value (>0.999) indicates that the pseudo-second-order equation satisfactorily describes the adsorption for each studied temperature. Many previous studies have reported that plots of the pseudo-second-order model converged better with experimental data.
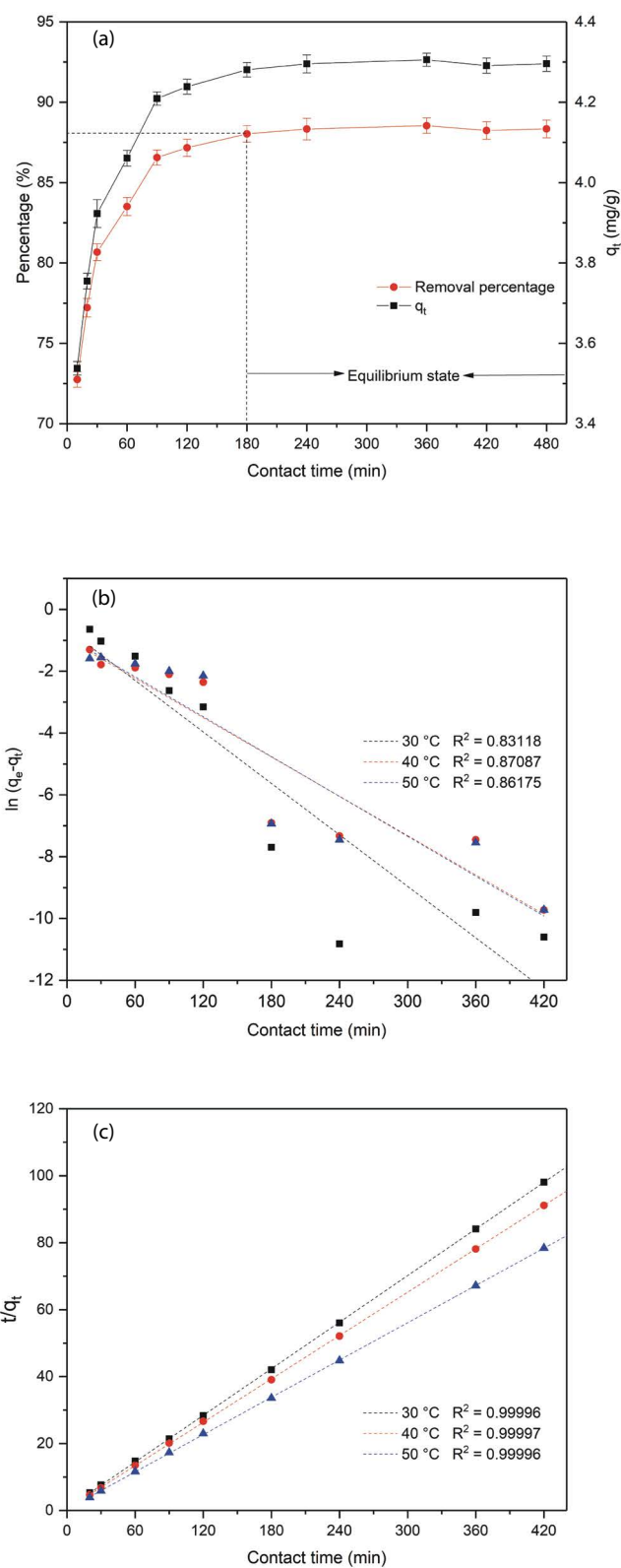

Fig. 9. Kinetic models for the adsorption of Sb(III) on Fe-ATP at different temperatures: (a) the effect of reaction time, (b) pseudo-first-order kinetics, and (c) pseudo-second-order kinetics.

Table 4
Adsorption kinetic parameters for the adsorption of Sb(III)

Temperature (°C)	$q_{e,exp}$ (mg/g)	Pseudo-first-order			Pseudo-second-order		
		K_1 (min^{-1})	$q_{e1,cal}$ (mg/g)	R^2	K_2 (g/mg/min)	$q_{e2,cal}$ (mg/g)	R^2
30	3.89	0.0113	0.33	0.83118	0.1625	3.85	0.99996
40	4.11	0.0089	0.27	0.87087	0.2394	4.05	0.99997
50	4.46	0.0062	0.24	0.86175	0.3003	4.37	0.99996

The R^2 values of the pseudo-first-order and pseudo-second-order models for Sb(III) adsorption by Mn-modified perlite were 0.935 and 0.999 at 303 K, respectively [51]. Zhao et al. [71] also found that the pseudo-second-order model described the adsorption of Sb acetate on sodium montmorillonite well.

The calculated q_e values (3.85–4.37 mg/g) according to the pseudo-second-order equation are close to 4.28 mg/g, indicating that the adsorption process is controlled by chemical processes. The valence forces through the exchange of electrons between Sb(III) and Fe-ATP are the main factor limiting the adsorption rate. This result further strengthens the conclusion that the adsorption of Sb(III) onto Fe-ATP progresses primarily via chemical ion exchange, according to the D–R isotherm, as shown in Section 3.4. The k_2 value is increased with increasing temperature, which means that increases in the temperature correspond to decreases in adsorption rate. However, the adsorption capacity is significantly increased from 3.89 to 4.46 mg/g as the temperature is increased from 30°C to 50°C. Therefore, the adsorption of Sb(III) onto Fe-ATP is endothermic, as can be concluded from Table 4. This result is consistent with that from the section on adsorption thermodynamics (Section 3.3).

Based on the earlier studies, the adsorption mechanism of Sb(III) on Fe-ATP was proposed as follows. Surface complexation and ion exchange reactions were suggested as the dominant mechanisms at lower pH, while electrostatic factors controlled the adsorption process under neutral or alkaline conditions. According to the Gibbs free energy, chemisorption was important in the adsorption process, consistent with the results from the kinetic models. The D–R model was also used to explore the adsorption mechanism. The mean free energy was 10 kJ/mol, implying that chemical ion exchange was the main factor affecting the adsorption process. The adsorption mechanism indicated that the Sb(III) was first adsorbed on the surface of Fe-ATP by electrostatic attraction, while further adsorption was attributed to chemisorption.

3.6. Desorption studies

The regeneration of the adsorbent is critical to render adsorption more economical and effective. Thus, it is necessary to investigate the reuse potential of Fe-ATP. The capability for desorption was defined as the percentage of Sb(III) desorbed over the total amount of Sb(III) adsorbed by Fe-ATP. In recent years, ethylenediaminetetraacetic acid (EDTA) and NaOH have been used as desorbents with strong chelating functions on heavy metals [72]. In this work, the adsorbed Sb(III) was eluted by treatment with 0.1 mol/L EDTA or 0.1 mol/L NaOH. As shown in Fig. 10, the capacity of
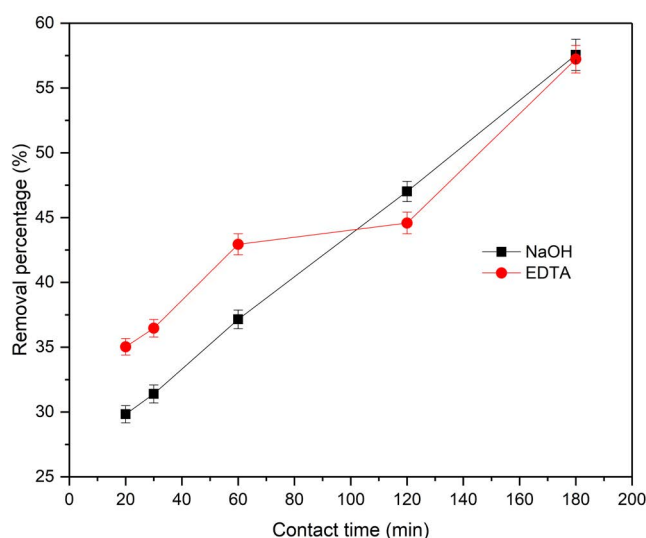

Fig. 10. The desorption kinetic curves of Sb(III) from Fe-ATP (T = 303 K, m = 50 mg, V = 25 mL).

desorption is approximately 60% for both EDTA and NaOH at 180 min. A large amount of Fe^{3+} is also released in the solution with EDTA, but only slight amounts are found with NaOH. The surface of Fe-ATP is negatively recharged and therefore unfavorable for adsorption because of the reaction between NaOH and Fe-ATP. This supports the decrease in removal percentage with increasing pH. Therefore, it is better to use EDTA as the desorbent.

The results clearly indicate that Fe-ATP can be used repeatedly in the practical treatment of Sb-contaminated water. The positive entropy value (93.9 J/mol K) obtained in Section 3.3 also shows that Fe-ATP has a strong affinity for Sb(III) and can be reused. Other eluents for desorption have been reported in previous studies. Ten adsorption/desorption cycles of Sb(III) on diatomite were performed and showed a slight decrease of approximately 3% in the adsorption yield [59]. Leng et al. [19] used EDTA as an eluent to perform experiments and demonstrated that the removal percentage for graphene remained at 60% after five successive cycles. Fan et al. [58] tested EDTA, HCl, and HNO$_3$ as eluents and found that the desorption efficiency with 3 mol/L HCl (96.7%) was much higher than that with 0.1 mol/L EDTA (2.8%).

4. Conclusions

In this study, a novel and efficient Fe-ATP adsorbent has been successfully synthesized and used for the removal of

Sb(III) from aqueous solutions. The effects of reaction time, pH, and coexisting ions on the adsorption process were investigated through batch adsorption experiments. It was clear that the adsorption was significantly influenced by pH and the capacity decreased with increasing pH. The adsorption isotherms were better described by the Freundlich model compared with the Langmuir and D–R models based on the R^2 values of 0.99045, 0.77596, and 0.96858, respectively. Adsorption thermodynamics were applied to study the thermal nature of the adsorption process. The adsorption of Sb(III) was higher at 323 K than at 303 K, according to the positive value of $\Delta H°$ (6.5 kJ/mol). The kinetics model demonstrated that the adsorption was relatively rapid, with the removal percentage exceeding 85% within 180 min. The pseudo-second-order model was more accurate in describing the adsorption process, implying the process was controlled by chemical adsorption. Furthermore, 0.1 mol/L of EDTA or NaOH was used as a desorbent in desorption studies, and the desorption percentage with both agents was approximately 60% after 180 min. This work demonstrates the potential use of Fe-ATP as an effective recyclable adsorbent for the low-cost and fast-uptake elimination of Sb from wastewater.

Acknowledgment

References

[1] M. Fomina, G.M. Gadd, Biosorption: current perspectives on concept, definition and application, Bioresour. Technol., 160 (2014) 3–14.

[2] F. Scinicariello, M.C. Buser, A.G. Feroe, R. Attanasio, Antimony and sleep-related disorders: NHANES 2005–2008, Environ. Res., 156 (2017) 247–252.

[3] M. Filella, N. Belzile, Y.W. Chen, Antimony in the environment: a review focused on natural waters: I. Occurrence, Earth Sci. Rev., 57 (2002) 125–176.

[4] Y.J. An, M. Kim, Effect of antimony on the microbial growth and the activities of soil enzymes, Chemosphere, 74 (2009) 654–659.

[5] J. Luo, C. Hu, X. Meng, J. Crittenden, J. Qu, P. Peng, Antimony removal from aqueous solution using novel α-MnO$_2$ nanofibers: equilibrium, kinetic and DFT studies, ACS Sustainable Chem. Eng., 5 (2017) 2255–2264.

[6] J. Li, B. Zheng, Y. He, Y. Zhou, X. Chen, S. Ruan, Y. Yang, C. Dai, L. Tang, Antimony contamination, consequences and removal techniques: a review, Ecotoxicol. Environ. Saf., 156 (2018) 125–134.

[7] C. Shan, Z. Ma, M. Tong, Efficient removal of trace antimony(III) through adsorption by hematite modified magnetic nanoparticles, J. Hazard. Mater., 268 (2014) 229–236.

[8] Z. Qi, T.P. Joshi, R. Liu, Y. Li, H. Liu, J. Qu, Adsorption combined with superconducting high gradient magnetic separation technique used for removal of arsenic and antimony, J. Hazard. Mater., 343 (2018) 36–48.

[9] J. Xi, M. He, C. Lin, Adsorption of antimony(V) on kaolinite as a function of pH, ionic strength and humic acid, Environ. Earth Sci., 60 (2010) 715–722.

[10] L. Paoli, E. Fiorini, S. Munzi, S. Sorbo, A. Basile, S. Loppi, Antimony toxicity in the lichen *Xanthoria parietina* (L.) Th. Fr, Chemosphere, 93 (2013) 2269–2275.

[11] Z. Wu, M. He, X. Guo, R. Zhou, Removal of antimony (III) and antimony (V) from drinking water by ferric chloride coagulation: competing ion effect and the mechanism analysis, Sep. Purif. Technol., 76 (2010) 184–190.

[12] M. Kang, M. Kawasaki, S. Tamada, T. Kamei, Y. Magara, Effect of pH on the removal of arsenic and antimony using reverse osmosis membranes, Desalination, 131 (2000) 293–298.

[13] A.S. Koparal, R. Özgür, Ü.B. Öğütveren, H. Bergmann, Antimony removal from model acid solutions by electrodeposition, Sep. Purif. Technol., 37 (2004) 107–116.

[14] J. Luo, X. Luo, J. Crittenden, J. Qu, Y. Bai, Y. Peng, J. Li, Removal of antimonite (Sb(III)) and antimonate (Sb(V)) from aqueous solution using carbon nanofibers that are Decorated with zirconium oxide (ZrO$_2$), Environ. Sci. Technol., 49 (2015) 11115–11124.

[15] S.Y. Nishiyama, K. Saito, K. Saito, K. Sugita, K. Sato, M. Akiba, T. Saito, S. Tsuneda, A. Hirata, M. Tamada, High-speed recovery of antimony using chelating porous hollow-fiber membrane, J. Membr. Sci., 214 (2003) 275–281.

[16] N.V. Kirichenko, A.I. Nikolaev, V.G. Maiorov, A.V. Tyuremnov, E.G. Il In, Extraction of antimony and tantalum from aqueous fluoride solutions by n-octanol and tributyl phosphate, Russ. J. Inorg. Chem., 58 (2013) 474–480.

[17] M. Xu, P. Yin, X. Liu, X. Dong, Q. Xu, R. Qu, Preparation, characterization, adsorption equilibrium, and kinetics for gold-ion adsorption of spent buckwheat hulls modified by organodiphosphonic acid, Ind. Eng. Chem. Res., 52 (2013) 8114–8124.

[18] A. Olgun, N. Atar, Equilibrium, thermodynamic and kinetic studies for the adsorption of lead(II) and nickel(II) onto clay mixture containing boron impurity, J. Ind. Eng. Chem., 18 (2012) 1751–1757.

[19] Y. Leng, W. Guo, S. Su, C. Yi, L. Xing, Removal of antimony(III) from aqueous solution by graphene as an adsorbent, Chem. Eng. J., 211–212 (2012) 406–411.

[20] T.A. Saleh, A. Sarı, M. Tuzen, Effective adsorption of antimony (III) from aqueous solutions by polyamide-graphene composite as a novel adsorbent, Chem. Eng. J., 307 (2016) 230–238.

[21] S. Rakshit, D. Sarkar, P. Punamiya, R. Datta, Antimony sorption at gibbsite-water interface, Chemosphere, 84 (2011) 480–483.

[22] V.K. Mittal, S. Bera, S.V. Narasimhan, S. Velmurugan, Sorption of Sb(III) on carbon steel surface in presence of molybdate and selenite in citric acid medium, Appl. Surf. Sci., 258 (2011) 1525–1530.

[23] J. Xi, M. He, K. Wang, G. Zhang, Adsorption of antimony(III) on goethite in the presence of competitive anions, J. Geochem. Explor., 132 (2013) 201–208.

[24] Y. Li, Z. Wang, X. Xie, J. Zhu, R. Li, T. Qin, Removal of Norfloxacin from aqueous solution by clay-biochar composite prepared from potato stem and natural attapulgite, Colloids Surf., A, 514 (2017) 126–136.

[25] Z. Jing, S. Xie, Y.S. Ho, Removal of fluoride ions from aqueous solution using modified attapulgite as adsorbent, J. Hazard. Mater., 165 (2009) 218–222.

[26] A. Zhou, J. Wang, Y. Lin, X. Guan, R. Zuo, Y. Teng, Adsorptive removal of trace uranium ions from simulated wastewater with FeCl3-modified attapulgite with sodium alginate beads, Desal. Wat. Treat., 107 (2018) 155–164.

[27] W. Wang, G. Tian, Z. Zhang, A. Wang, A simple hydrothermal approach to modify palygorskite for high-efficient adsorption of Methylene blue and Cu(II) ions, Chem. Eng. J., 265 (2015) 228–238.

[28] J. Xu, W. Wang, J. Gao, A. Wang, J. Xu, W. Wang, J. Gao, A. Wang, Fabrication of stable glycine/palygorskite nanohybrid via high-pressure homogenization as high-efficient adsorbent for Cs(I) and Methyl violet, J. Taiwan Inst. Chem. E, 80 (2017) 997–1005.

[29] R. Yang, D. Li, A. Li, H. Yang, Adsorption properties and mechanisms of palygorskite for removal of various ionic dyes from water, Appl. Clay Sci., 151 (2018) 20–28.

[30] G. Tian, W. Wang, Z. Li, Y. Kang, A. Wang, A functionalized hybrid silicate adsorbent derived from naturally abundant low-grade palygorskite clay for highly efficient removal of hazardous antibiotics, Chem. Eng. J., 293 (2016) 376–385.

[31] G. Tian, W. Wang, B. Mu, Y. Kang, A. Wang, Facile fabrication of carbon/attapulgite composite for bleaching of palm oil, J. Taiwan Inst. Chem. Eng., 50 (2015) 252–258.

[32] H. Yin, X. Yan, X. Gu, Evaluation of thermally-modified calcium-rich attapulgite as a low-cost substrate for rapid phosphorus removal in constructed wetlands, Water Res., 115 (2017) 329–338.

[33] N. Sun, Y. Zhang, L. Ma, S. Yu, J. Li, Preparation and characterization of chitosan/purified attapulgite composite for sharp adsorption of humic acid from aqueous solution at low temperature, J. Taiwan Inst. Chem. Eng., 78 (2017) 96–103.

[34] S. Li, Y. Wei, Y. Kong, Y. Tao, C. Yao, R. Zhou, Electrochemical removal of lead ions using paper electrode of polyaniline/attapulgite composites, Synth. Met., 199 (2015) 45–50.

[35] Q. Fan, L. Zhan, H. Zhao, Z. Jia, J. Xu, W. Wu, Adsorption of Pb(II) on palygorskite from aqueous solution: effects of pH, ionic strength and temperature., Appl. Clay Sci., 45 (2009) 111–116.

[36] H. Cui, Y. Qian, Q. Li, Z. Wei, J. Zhai, Fast removal of Hg(II) ions from aqueous solution by amine-modified attapulgite, Appl. Clay Sci., 72 (2013) 84–90.

[37] N. Guo, J. Wang, J. Li, Y. Teng, Y. Zhai, Dynamic adsorption of Cd^{2+} onto acid-modified attapulgite from aqueous solution, Clays Clay Miner., 62 (2014) 415–424.

[38] H. Han, C. Cheng, S. Hu, X. Li, W. Wang, C. Xiao, Z. Xu, D. Shao, Facile synthesis of gelatin modified attapulgite for the uptake of uranium from aqueous solution, J. Mol. Liq., 234 (2017) 172–178.

[39] A.K. Leuz, H. Mönch, C.A. Johnson, Sorption of Sb(III) and Sb(V) to goethite: influence on Sb(III) oxidation and mobilization., Environ. Sci. Technol., 40 (2006) 7277–7282.

[40] K. Nithya, A. Sathish, P. Senthil Kumar, T. Ramachandran, Fast kinetics and high adsorption capacity of green extract capped superparamagnetic iron oxide nanoparticles for the adsorption of Ni(II) ions, J. Ind. Eng. Chem., 59 (2018) 230–241.

[41] A. Kasiuliene, I. Carabante, P. Bhattacharya, A.G. Caporale, P. Adamo, J. Kumpiene, Removal of metal(oid)s from contaminated water using iron-coated peat sorbent, Chemosphere, 198 (2018) 290–296.

[42] M.S. Islam, W.S. Choi, B. Nam, C. Yoon, H. Lee, Needle-like iron oxide@$CaCO_3$ adsorbents for ultrafast removal of anionic and cationic heavy metal ions, Chem. Eng. J., 307 (2017) 208–219.

[43] C. Zhang, Z. Yu, G. Zeng, B. Huang, H. Dong, J. Huang, Z. Yang, J. Wei, L. Hu, Q. Zhang, Phase transformation of crystalline iron oxides and their adsorption abilities for Pb and Cd, Chem. Eng. J., 284 (2016) 247–259.

[44] C. Rémazeilles, P. Refait, On the formation of β-FeOOH (akaganéite) in chloride-containing environments, Corros. Sci., 49 (2007) 844–857.

[45] D.N. Bakoyannakis, E.A. Deliyanni, A.I. Zouboulis, K.A. Matis, L. Nalbandian, T. Kehagias, Akaganeite and goethite-type nanocrystals: synthesis and characterization, Microporous Mesoporous Mater., 59 (2003) 35–42.

[46] M. Li, Z. Wu, H. Kao, Study on preparation, structure and thermal energy storage property of capric–palmitic acid/attapulgite composite phase change materials, Appl. Energy, 88 (2011) 3125–3132.

[47] C. Chen, X. Wang, Sorption of Th (IV) to silica as a function of pH, humic/fulvic acid, ionic strength, electrolyte type., Appl. Radiat. Isot., 65 (2007) 155–163.

[48] R. Watkins, D. Weiss, W. Dubbin, K. Peel, B. Coles, T. Arnold, Investigations into the kinetics and thermodynamics of Sb(III) adsorption on goethite (α-FeOOH), J. Colloid Interface Sci., 303 (2006) 639–646.

[49] V.K. Mittal, S. Bera, S.V. Narasimhan, S. Velmurugan, Adsorption behavior of antimony(III) oxyanions on magnetite surface in aqueous organic acid environment, Appl. Surf. Sci., 266 (2013) 272–279.

[50] Y. Inoue, M. Munemori, The coprecipitation of antimony(III or V) with iron(III) hydroxide, Bull. Chem. Soc. Jpn., 53 (1980) 926–929.

[51] A. Sarı, G. Şahinoğlu, M. Tüzen, Antimony(III) Adsorption from aqueous solution using raw perlite and Mn-modified perlite: equilibrium, thermodynamic, and kinetic studies, Ind. Eng. Chem. Res., 51 (2012) 6877–6886.

[52] M. Villalobos, J.O. Leckie, Carbonate adsorption on goethite under closed and open CO_2 conditions, Geochim. Cosmochim. Acta, 64 (2000) 3787–3802.

[53] H. Cui, Q. Yan, Q. Li, Q. Zhang, J. Zhai, Adsorption of aqueous Hg(II) by a polyaniline/attapulgite composite, Chem. Eng. J., 211–212 (2012) 216–223.

[54] J. Xi, M. He, C. Lin, Adsorption of antimony(III) and antimony(V) on bentonite: kinetics, thermodynamics and anion competition, Microchem. J., 97 (2011) 85–91.

[55] C. Zhang, Y. Li, F. Wang, Z. Yu, J. Wei, Z. Yang, C. Ma, Z. Li, Z.Y. Xu, G. Zeng, Performance of magnetic zirconium-iron oxide nanoparticle in the removal of phosphate from aqueous solution, Appl. Surf. Sci., 396 (2017) 1783–1792.

[56] I.P. Okoye, C. Obi, Thermodynamic and kinetic evaluations of some heavy metal ions on aluminum-pillared and unpillared bentonite clays, Int. Arch. Appl. Sci. Technol., 3 (2012) 58–67.

[57] T.K. Naiya, A.K. Bhattacharya, S. Mandal, S.K. Das, The sorption of lead(II) ions on rice husk ash, J. Hazard. Mater., 163 (2009) 1254–1264.

[58] H. Fan, W. Sun, B. Jiang, Q. Wang, D. Li, C. Huang, K. Wang, Z. Zhang, W. Li, Adsorption of antimony(III) from aqueous solution by mercapto-functionalized silica-supported organic–inorganic hybrid sorbent: mechanism insights, Chem. Eng. J., 286 (2016) 128–138.

[59] A. Sarı, D. ÇItak, M. Tuzen, Equilibrium, thermodynamic and kinetic studies on adsorption of Sb(III) from aqueous solution using low-cost natural diatomite., Chem. Eng. J., 162 (2010) 521–527.

[60] N.V. Deorkar, L.L. Tavlarides, A chemically bonded adsorbent for separation of antimony, copper and lead, Hydrometallurgy, 46 (1997) 121–135.

[61] F. Shakerian, S. Dadfarnia, A.M.H. Shabani, M.N.A. Abadi, Synthesis and characterisation of nano-pore antimony imprinted polymer and its use in the extraction and determination of antimony in water and fruit juice samples, Food Chem., 145 (2014) 571–577.

[62] P. Thanabalasingam, W.F. Pickering, Specific sorption of antimony (III) by the hydrous oxides of Mn, Fe, and Al, Water Air Soil Pollut., 49 (1990) 175–185.

[63] D. Mendil, H. Bardak, M. Tuzen, M. Soylak, Selective speciation of inorganic antimony on tetraethylenepentamine bonded silica gel column and its determination by graphite furnace atomic absorption spectrometry, Talanta, 107 (2013) 162–166.

[64] H. Fan, Y. Sun, Q. Tang, W. Li, T. Sun, Selective adsorption of antimony(III) from aqueous solution by ion-imprinted organic–inorganic hybrid sorbent: kinetics, isotherms and thermodynamics, J. Taiwan Inst. Chem. Eng., 45 (2014) 2640–2648.

[65] G. Ungureanu, C. Filote, S.C.R. Santos, A.R.B. Rui, I. Volf, C.M.S. Botelho, Antimony oxyanions uptake by green marine macroalgae, J. Environ. Chem. Eng., 4 (2016) 3441–3450.

[66] M.A. Salam, R.M. Mohamed, Removal of antimony (III) by multi-walled carbon nanotubes from model solution and environmental samples, Chem. Eng. Res. Des., 91 (2013) 1352–1360.

[67] G. Ungureanu, S. Santos, B. Rui, C. Botelho, Biosorption of antimony by brown algae *S. muticum* and *A. nodosum*, Environ. Eng. Manage. J., 14 (2015) 455–463.

[68] F. Wu, F. Sun, S. Wu, Y. Yan, B. Xing, Removal of antimony(III) from aqueous solution by freshwater cyanobacteria *Microcystis* biomass, Chem. Eng. J., 183 (2012) 172–179.

[69] H. Fan, Q. Tang, Y. Sun, Z. Zhang, W. Li, Selective removal of antimony(III) from aqueous solution using antimony(III)-imprinted organic–inorganic hybrid sorbents by combination of surface imprinting technique with sol–gel process, Chem. Eng. J., 258 (2014) 146–156.

[70] T. Yu, C. Zeng, M. Ye, Y. Shao, The adsorption of Sb(III) in aqueous solution by Fe_2O_3-modified carbon nanotubes, Water Sci. Technol., 68 (2013) 658–664.

[71] Z. Zhao, X. Wang, C. Zhao, X. Zhu, S. Du, Adsorption and desorption of antimony acetate on sodium montmorillonite, J. Colloid Interface Sci., 345 (2010) 154–159.

[72] N. Li, L. Zhang, Y. Chen, Y. Tian, H. Wang, Adsorption behavior of Cu(II) onto titanate nanofibers prepared by alkali treatment., J. Hazard. Mater., 189 (2011) 265–272.